Decomposition and Hydrocarbon Growth Processes for Esters in Non-Premixed Flames†

William R. Schwartz,* Charles S. McEnally, and Lisa D. Pfefferle

Department of Chemical Engineering and Center for Combustion Studies, Yale University, New Haven, Connecticut 06520-8286

Received: September 1, 2005

Biomass fuels are a promising renewable energy source, and so, the mechanisms that may produce toxic oxygenated byproducts and aromatic hydrocarbons from oxygenated hydrocarbons are of interest. Esters have the form R−(C═O)−O−R′ and are components of biodiesel fuels. The five specific esters studied here are isomers of $C_5H_{10}O_2$. The experiments were performed in atmospheric pressure coflowing methane/air non-premixed flames. A series of flames were generated by separately doping the fuel mixture with 5 000 ppm of each ester. This concentration is sufficiently large to produce measurable changes in intermediate hydrocarbon concentrations, yet small enough to not disturb the overall flame structure. Since the overall structure is not perturbed, the measured changes in the intermediate hydrocarbons can be directly attributed to the reactions of the esters. Analysis of these changes reveals that unimolecular six-centered dissociation is the primary decomposition pathway for the three esters with molecular arrangements capable of undergoing that mechanism. The remaining two esters exhibited decomposition rates and products that are consistent with simple fission as the dominant decomposition mechanism, though we do not exclude other pathways from playing a significant role in their decomposition. All of the esters produce aromatic hydrocarbons at higher rates than the undoped fuel, and the molecular arrangement of the ester isomers plays a role in the degree of aromatic formation. Isomer variations also influence the type and quantity of toxic oxygenates that are produced in the flames.

Introduction

This paper describes our investigation of the five isomers of $C_5H_{10}O_2$ esters (R−CO−O−R′), which is part of a broader study of the chemical mechanisms that are responsible for fuel decomposition and aromatic hydrocarbon production from oxygenated hydrocarbons in soot-producing flames. Previous studies have covered butyl alcohols (C_4H_9OH) and alkyl ethers (R−O−R′).[1,2]

Oxygenated hydrocarbons are major constituents of biomass fuels, which are receiving increased attention as a renewable energy source. Some of the technical issues associated with oxygen-containing fuels are their ability to reduce particulate emissions[3] and their propensity to form toxic byproducts such as aldehydes.[4,5] A fundamental understanding of oxygenate combustion chemistry is necessary to fully exploit the former and minimize the latter.

Esters are of particular interest, since they are a major component of biodiesel fuels. Typical biodiesel fuels consist of mixtures of saturated and unsaturated methyl esters containing carbon chains of twelve or more atoms in length.[6] The $C_5H_{10}O_2$ esters were chosen for this study to limit the number of possible decomposition products to a manageable level and to focus on the basic building blocks involved in soot formation.

This investigation focuses on the analysis of experimental data from ester combustion in coflowing non-premixed flames. Such flames are typical of many practical combustors, especially soot-producing systems such as diesel engines and gas turbines, yet are simple enough to permit basic understanding. For example, the flames can be modeled with detailed chemical kinetic mechanisms.[7−9] Fisher et al. have developed a detailed chemical kinetic model for the combustion of methyl butanoate,[10] one of the esters included in this investigation. However, experimental data from flames have not been available to test this model.

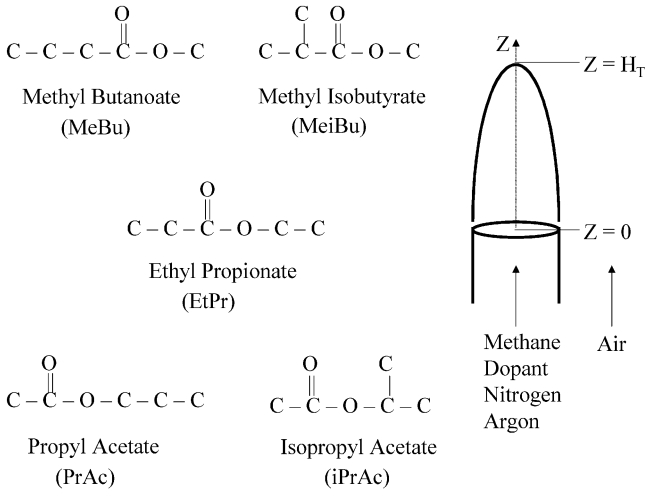

Figure 1. The five ester isomers of $C_5H_{10}O_2$ were separately added to the fuel of a coflowing non-premixed flame. The left side shows the structure of the dopants and assigns them abbreviations, while the right side shows a schematic of the flame geometry. $Z = H_T$ is the height above the burner surface where the centerline temperature peaks, which is a good surrogate to the height where the stoichiometric flame front intersects the centerline.[7]

We studied CH_4/air coflowing non-premixed flames whose fuel was separately doped with 5 000 ppm of the investigated esters. Figure 1 shows the structure of the dopants and assigns them abbreviations. Stable C3−C12 hydrocarbons, major spe-

† Part of the special issue "David M. Golden Festschrift".

* Corresponding author. Fax: 203-432-4387. Phone: 203-432-4059. E-mail: william.schwartz@yale.edu.

10.1021/jp0549576 CCC: $33.50
Published on Web 12/10/2005

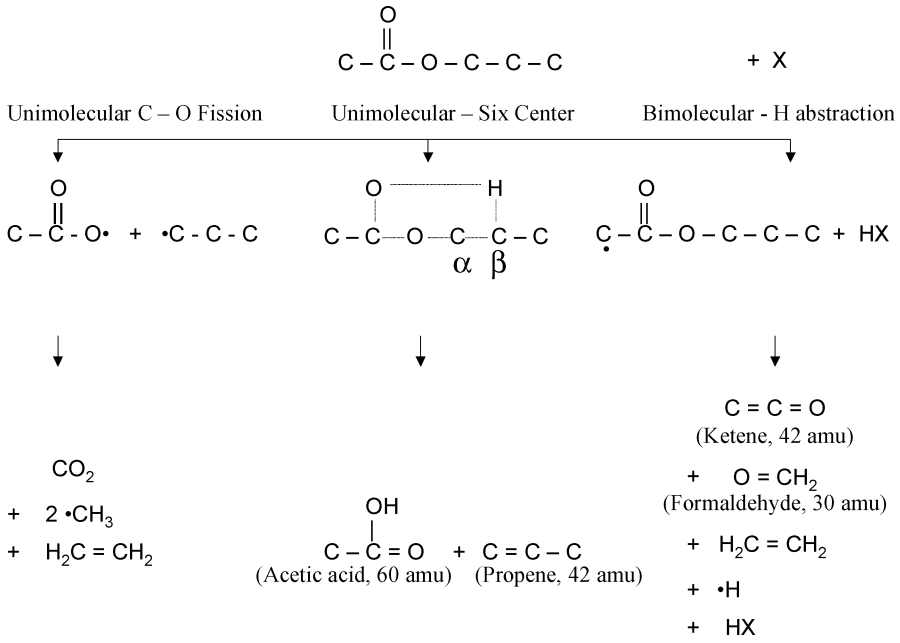

Figure 2. Esters can potentially decompose by three pathways, which are shown here for the specific case of PrAc. The simple fission reaction is illustrated for the dissociation of the C−O bond. The bimolecular H-abstraction reaction is illustrated for abstraction of the terminal H atom on the carbon adjacent to the carbonyl group.

cies, and temperature were measured on the centerline of each flame. Each of the esters was investigated in flames with virtually identical major species and temperature profiles. This ensured that the differences in the identities and concentrations of measured products were caused by the structure of the ester dopant. Comparison of fuels whose structures vary systematically is an established method for identifying kinetic pathways (e.g., ref 11).

In general, hydrocarbons in flames can decompose by bimolecular H abstraction or by unimolecular reactions. Unimolecular reactions are divided into simple fission (one bond breaks) and complex fission (multiple bonds break and form). Each of these mechanisms is illustrated for PrAc in Figure 2.

The simple fission illustration shows the C−O bond breaking, which creates two radicals at the location where the bond is broken. A β-scission reaction follows, whereby the weakest bond on the atom adjacent to the radical breaks, and a double bond is formed. Thus, the fragment containing the O radical dissociates to form CO_2 plus methane radical, and the fragment containing the C radical dissociates to form ethene plus methane radical.

The H-abstraction illustration shows a bimolecular interaction whereby the H atom on the terminal C atom adjacent to the carbonyl group is abstracted from the ester, and a radical is formed at the abstraction site. As in the simple fission process, a β-scission reaction follows, and the radical site is converted to a double bond. For PrAc, the β-scission reaction also results in the formation of another radical, causing additional β-scission reactions to occur. Further decomposition products are ketene, formaldehyde, ethene, plus a hydrogen radical that will react with other molecules.

The complex fission illustration represents a six-centered dissociation reaction that produces a carboxylic acid and an alkene. The six-centered dissociation reaction involves the formation of an intermediate ring, which includes the single-bond O atom, the α C atom bonded to the single-bond O atom, a β C atom, one of the H atoms bonded to the β C atom, and the carbonyl group. During a concerted process, an OH bond forms, and the molecule breaks to form the carboxylic acid and the alkene. For PrAc, these decomposition products are acetic acid and propene. The six-centered dissociation reaction is the dominant complex fission reaction mechanism for alkyl esters.[12]

TABLE 1: Fuel Components and Flow Rates Used to Generate Flames with Consistent Profiles

fuel mixture	dopant mole fraction (ppm)	methane flow rate (cc/min)	N_2 + Ar flow rate (cc/min)	air flow rate (cc/min)
undoped		330	330	44 000
EtPr	5000	327	330	44 000
*i*PrAc	5000	327	330	44 000
MeBu	5000	327	330	44 000
Me*i*Bu	5000	327	330	44 000
PrAc	5000	327	330	44 000

The objectives of our investigation are as follows: (1) to determine the relative importance of the unimolecular and bimolecular ester decomposition pathways in non-premixed flames; (2) to identify the intermediates formed from esters; and (3) to analyze the effect of ester structure on the degree of aromatic hydrocarbon and oxygenated hydrocarbon formation.

Experimental Methods

We used the same equipment and procedures as in our earlier studies of oxygenated hydrocarbons.[1] Under atmospheric pressure, coflowing laminar non-premixed flames were generated with a burner in which the fuel mixture flows out of an 11-mm-diameter tube and reacts with air that flows from the annular region outside this tube. The right side of Figure 1 illustrates this geometry.

The fuel mixture, which consisted of CH_4, N_2, and Ar, was doped with a small amount of one particular ester. Each of the ester dopants was studied in separate flames. The fuel component flow rates are shown in Table 1. The flow rates were chosen so that (1) the dopant concentration in the fuel equals 5000 ppm, (2) the carbon flux was constant, (3) the ratio of N_2 plus Ar to hydrocarbons was constant, and (4) the Ar concentration was constant. Conditions (2) and (3), combined with low dopant concentration, produced flames with indistinguishable heights, temperatures, and major species profiles. Condition (4) created

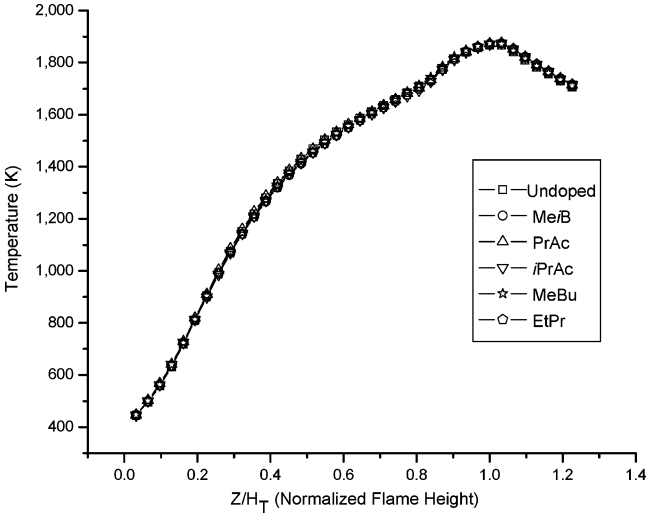

Figure 3. Centerline gas temperature (T_g) vs normalized flame height (Z/H_T). Temperatures were measured with thermocouples.[14]

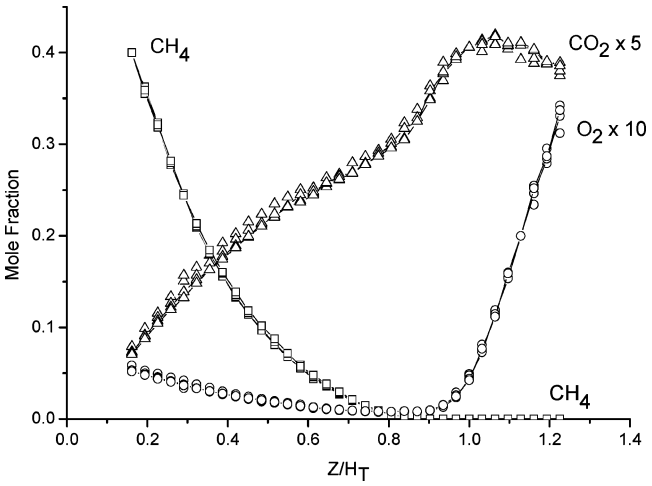

Figure 4. Centerline mole fraction of the major flame species CH_4, CO_2, and O_2 were measured with electron impact mass spectrometry.

an internal standard that was used to relate species density in the diagnostic apparatus with species concentration in the flame.[13]

Gas temperatures, T_g, were measured with a thermocouple,[14] major species were measured with electron impact mass spectrometry, and C3−C12 hydrocarbons were measured with 118-nm photoionization mass spectrometry.[13] The magnitude of the uncertainty in the measurements depends on the property being measured and the location in the flame, but upper limits to the relative and absolute uncertainties have been established in prior studies using the same experimental procedures and apparatus.[1] Conservative upper limits to the relative and absolute uncertainties are ±10% and ±65 K (T_g) and ±10% and +100%/−50% (species concentration). All measurements were made on the burner centerline.

Results and Discussion

Figures 3 and 4 show temperature and major species concentrations for each of the flames as a function of a normalized flame height, Z/H_T. Z is the dimensional height above the burner surface, and H_T is the Z value at the centerline peak temperature. The temperature and major species measurements reveal that the ester dopants did not affect the overall flame structure. Therefore, the dopant-to-dopant differences in decomposition rates and product concentrations are directly attributable to the rate parameters of the dopant decomposition and hydrocarbon growth pathways.

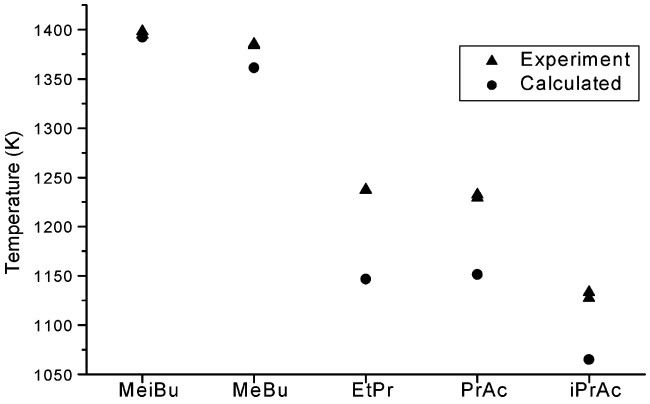

Figure 5. $T_{g1\%}$ experimental and calculated values. Differences in the decomposition rates reflect differing decomposition pathways. Variations between experimental and calculated values are within 8%.

Decomposition Rates. We characterize the disappearance rate of the fuel dopants with the parameter $T_{g1\%}$,[15] which is the centerline flame temperature that corresponds to a dopant concentration of 1% of the initial amount, or 50 ppm. $T_{g1\%}$ depends on the dopant decomposition rates and reflects the relative importance of the possible decomposition pathways shown in Figure 2. Lower values of $T_{g1\%}$ correspond to faster decomposition rates.

Figure 5 shows both measured and calculated values of $T_{g1\%}$ for each of the ester dopants. Two sets of experimental data were generated for each of the ester-doped flames. The corresponding measured values of $T_{g1\%}$ agreed within 0.5%.

We observe in Figure 5 that the esters fall into three distinct decomposition rate categories, with MeBu and Me*i*Bu having the slowest rates, *i*PrAc having the fastest rate, and EtPr and PrAc having intermediate rates. The relatively fast decomposition rates for *i*PrAc, EtPr, and PrAc are inconsistent with bimolecular H-atom abstraction as their primary decomposition pathway, but are consistent with unimolecular six-centered dissociation reactions. If bimolecular H-atom abstractions were the primary pathway for these esters, their decomposition rates would be comparable to MeBu and Me*i*Bu, the slowest decomposing esters in the group, since all of the alkyl ester dopants have similar C−H bond energies.[16]

The observation in Figure 5 that *i*PrAc decomposes at a faster rate than PrAc and EtPr is related to carbon branching on the carbon singly bonded to oxygen. First, carbon branching allows three or four additional H atoms to participate in the six-centered dissociation reaction for *i*PrAc. Second, the substituent branching effect has been shown to reduce the activation energy for ester six-centered dissociation reactions by 3.0−5.5 kcal/CH_3,[17] consistent with our observations.

The calculated values of $T_{g1\%}$ in Figure 5 are based on the assumption that unimolecular dissociation is the only consumption process and $d[E]/dt = k[E]$, where [E] is the ester dopant concentration and k is the temperature-dependent rate constant. The rate constants for each of the esters were obtained from prior studies, with the EtPr, PrAc, and *i*PrAc rate constants being for six-centered dissociation reactions[18−20] and the MeBu and Me*i*Bu rate constants being for simple fission reactions.[10,16] MeBu and Me*i*Bu cannot undergo six-centered dissociation reactions, because the chain that includes the carbonyl group, the single-bonded oxygen atom, and the methyl group is not large enough to form an intermediate six-membered ring. The

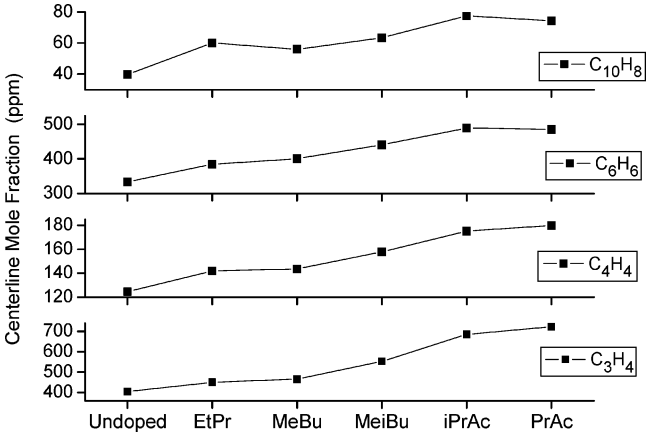

Figure 6. Maximum centerline product concentrations for C_3H_4, C_4H_4, C_6H_6 (benzene), and $C_{10}H_8$ (naphthalene).

calculated simple fission rates for MeBu and Me*i*Bu shown in Figure 5 agree with the measured experimental values to within 2%. This, however, does not rule out other mechanisms as important in their decomposition. The calculated six-centered dissociation rates for EtPr, PrAc, and *i*PrAc agree with the measured experimental values to within 8%.

Product Formation. The hydrocarbon and oxygenated hydrocarbon products are of interest, since they include air toxics[5] and aromatics that are precursors to soot formation.[21] About 25 hydrocarbons and oxygenated hydrocarbons were detectable in the size range of our sampling system. Centerline profiles of each species were measured in all 6 flames included in these experiments, though only portions of the results are presented here. The complete results are available from the corresponding author by request.

The 118-nm laser light used in this study has photon energy of 10.5 eV, which exceeds the ionization energies of all C3 and larger hydrocarbons except propane and butane.[22] Additionally, ketene (CH_2CO), acetaldehyde (CH_3CHO), plus C3 and larger oxygenated hydrocarbons have ionization energies less than 10.5 eV. Thus, the photoionization technique used in this study allowed us to measure centerline mole fraction profiles for most hydrocarbons and oxygenated hydrocarbons with molecular weights of 40−150 amu. Since the diagnostic technique is mass spectrometry, we cannot directly distinguish between different isomers of each product. However, we can often deduce specific isomers by analyzing reaction pathways and noting product spatial locations (e.g., Figure 8).

Figure 6 shows the maximum concentrations of C_3H_4, C_4H_4, and the aromatics benzene and naphthalene produced from the esters. C_3H_4 and C_4H_4 are included in the figure, because they have been shown to be fairly good surrogates to C_3H_3 and *n*-C_4H_3 radicals,[23] and these radicals are precursors to the formation of benzene and subsequently naphthalene.[24,25] We observe that the esters contribute to the formation of aromatics in the following order: *i*PrAc and PrAc > Me*i*Bu > EtPr and MeBu. We also observe that the formation of C_3H_4 and C_4H_4 correlate with the formation of the aromatics. Since these aromatics are soot precursors, the relative magnitudes of the peak concentrations shown in Figure 6 suggest the order of soot formation.

Figure 7 shows the centerline concentrations for propene (42 amu). Propene shows the highest concentration profiles of all the hydrocarbon decomposition species between 40 and 150 amu. The highest concentrations of propene are produced from PrAc and *i*PrAc and occur early in the flame (Z/H_T < 0.4 in Figure 7). This is in agreement with the predicted direct

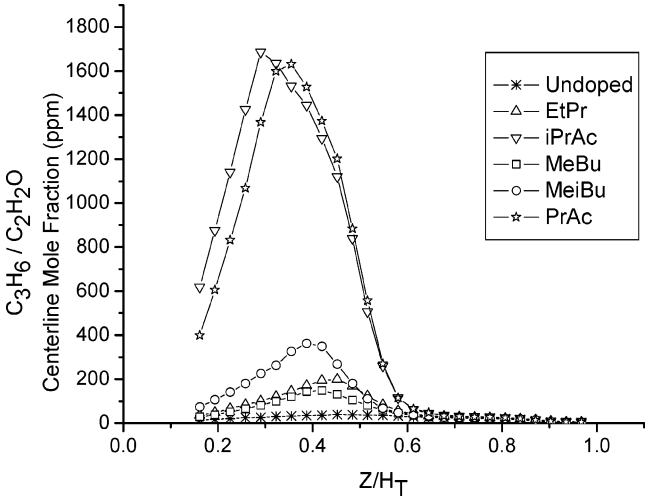

Figure 7. C_3H_6 (propene)/C_2H_2O (ketene) centerline mole fractions.

formation of propene via the six-centered dissociation reaction mechanism, which occurs more rapidly than simple fission or bimolecular H-atom abstraction (see Figure 5).

The next highest propene concentration shown in Figure 7 is produced from Me*i*Bu. Me*i*Bu can produce propene directly through either simple fission or H-atom abstraction reactions. However, only a limited number of simple fission or H-atom abstraction reactions will lead to direct propene formation. For example, only two of the five C−C and C−O bonds that could break during simple fission will result in the direct formation of propene. For H-atom abstraction, only six of the ten H atoms that could be lost from Me*i*Bu will result in the direct formation of propene.

MeBu and EtPr produce the lowest concentrations of propene. For these esters, the pathways to form propene are more limited. MeBu will only produce propene if H-atom abstraction occurs on the secondary carbon next to the terminal carbon or if secondary C1 and C2 addition reactions occur. Last, EtPr does not dissociate to form propene directly, and the peak at 42 amu may be due to the formation of ketene by simple fission (see Figure 2) or to secondary C1 and C2 addition reactions that can form propene. Note in Figure 7 that the peak concentration in the EtPr-doped flame lags behind the peak concentration found in the other flames. This suggests that secondary reactions may be involved in the production of propene or ketene from EtPr.

The peak concentrations of propene shown in Figure 7 correlate with the peak concentration of soot precursors shown in Figure 6, with PrAc and *i*PrAc producing the highest concentrations of both propene and soot precursors, followed by Me*i*Bu and then EtPr and MeBu. A correlation between propene and soot precursor concentrations was previously demonstrated in heptane-doped flames.[26] The connection between propene and soot formation is through the propargyl radical, C_3H_3. Propene may decompose by both C−H simple fission or H-atom abstraction to form propadiene (C_3H_4) and subsequently the benzene precursor propargyl radical (C_3H_3).

Figure 8 shows the centerline product concentrations for species with molecular weight of 74 amu. The first peak, occurring early in the flame, is produced solely by EtPr. The only mechanism that is consistent with this experimental result is the six-centered dissociation reaction whereby EtPr decomposes to form $C_3H_6O_2$ in the form of propanoic acid (CH_3CH_2-COOH). The second peak is produced in all of the flames, and the ester-doped flames have the same peak height as the undoped

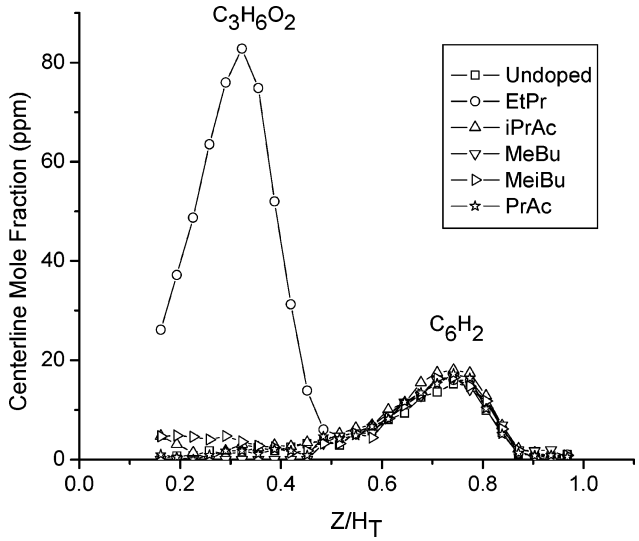

Figure 8. Centerline mole fraction profile for species of 74 amu.

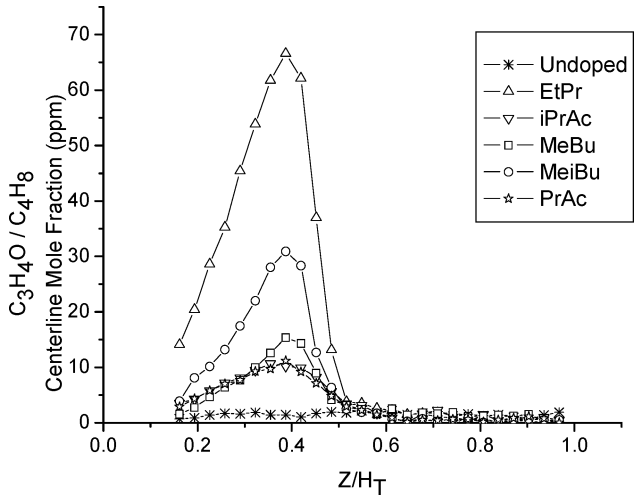

Figure 9. Centerline mole fraction profile for species of 56 amu.

flame. This suggests that the presence of the ester dopants is unrelated to the second peak. C_6H_2 is an expected secondary product from methane combustion, which is consistent with this second maximum concentration peak occurring late in the flame ($Z/H_T \approx 0.75$).

In addition to propanoic acid, several other oxygenated hydrocarbons are formed from ester combustion. Figure 9 shows centerline product concentrations for species with a molecular weight of 56 amu. The highest concentrations at this molecular weight are attributable to EtPr. We observed in Figure 8 that EtPr decomposes to propanoic acid via the six-centered dissociation reaction. Propanoic acid further decomposes to CH_3CHCO (56 amu) plus water. Note that the peak concentration of propanoic acid (Figure 8) occurs earlier in the flame than the peak concentration of CH_3CHCO (Figure 9). The normalized flame height, Z/H_T, is about 0.35 for propanoic acid and about 0.40 for CH_3CHCO. Thus, the formation of CH_3CHCO is consistent with the decomposition of EtPr via the six-centered dissociation reaction. We note that CH_3CHCO may also be formed directly from EtPr via bimolecular H-atom abstraction. C_4H_8, as well as CH_3CHCO, has a molecular weight of 56 amu. However, there is no structural mechanism for the esters to decompose to C4 hydrocarbons, so we conclude that C_4H_8 does not contribute to the peaks shown in Figure 9.

Figure 10 shows the centerline product concentrations for species with a molecular weight of 70 amu. MeBu and Me*i*Bu

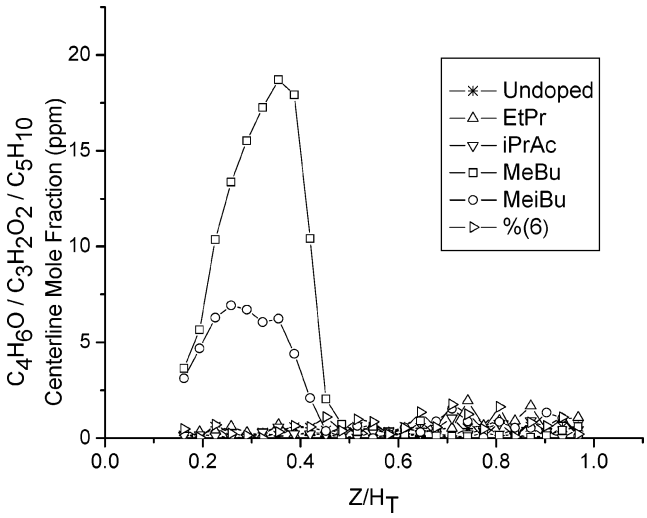

Figure 10. Centerline mole fraction profile for species of 70 amu.

are the only esters that form products at 70 amu. MeBu can directly decompose to CH_3CH_2CHCO by a four-centered reaction pathway, while Me*i*Bu can directly decompose to $(CH_3)_2CCO$ by either bimolecular H-atom abstraction or a four-centered reaction pathway. Under flame conditions, multiple reaction pathways are expected, and the relatively low concentration levels shown in Figure 10 are consistent with both H-atom abstraction and four-centered reactions being minor pathways.

MeBu and/or Me*i*Bu are also primary esters that form products with molecular weights of 54, 66, 68, and 86 amu, all of which include oxygenated hydrocarbons. Recall that MeBu and Me*i*Bu cannot undergo six-centered dissociation reactions and have the slowest decomposition rates (Figure 5). MeBu and Me*i*Bu persist with higher concentrations at higher flame heights, with increased flame temperature (Figure 3). With higher thermal energy, a greater variety of reaction pathways become significant, accounting for the greater variety of decomposition products in comparison to the products formed from the other ester isomers that can undergo six-centered dissociation reactions.

Concluding Remarks

The primary decomposition pathway for PrAc, *i*PrAc, and EtPr was determined to be a unimolecular six-centered dissociation reaction. MeBu and Me*i*Bu, which cannot undergo a six-centered dissociation reaction, have decomposition rates that are consistent with a unimolecular simple fission mechanism.

Propene was found to be a major decomposition product, whose presence correlates to the formation of aromatics and soot via propene decomposition to propargyl radicals. The degree of propene and aromatic hydrocarbon formation is dependent on the molecular structure of the ester fuel and the decomposition mechanism, with EtPr and MeBu showing the lowest concentrations of these products. The variety of oxygenated hydrocarbon products is also dependent on the structure of the ester fuel, with PrAc and *i*Prac producing the lowest variety of oxygenated hydrocarbons because of their high conversion to propene and acetic acid.

Acknowledgment. We thank the National Science Foundation for their financial support of this work. We also gratefully acknowledge useful discussions with William J. Pitz of the Lawrence Livermore National Laboratory.

References and Notes

(1) McEnally, C. S.; Pfefferle, L. D. *Proc. Combust. Inst*. **2005**, *30*, 1363−1370.
(2) McEnally, C. S.; Pfefferle, L. D. *Int. J. Chem. Kinet*. **2004**, *36*, 345−358.
(3) Beatrice, C.; Bertoli, C.; Giacomo, N. D. *Combust. Sci. Technol*. **1998**, *137*, 31−50.
(4) Wagner, T.; Wyszynski, M. *Proc. Inst. Mech. Eng.: J. Automob. Eng*. **1996**, *210*, 109−122.
(5) Koshland, C. P. *Proc. Combust. Inst*. **1996**, *26*, 2049−2065.
(6) Graboski, M.; McCormick, R. *Prog. Energy Combust. Sci*. **1998**, *24*, 125−164.
(7) Bennett, B. A. V.; McEnally, C. S.; Pfefferle, L. D.; Smooke, M. D. *Combust. Flame* **2000**, *123*, 522−546.
(8) D'Anna, A.; Kent, J. H. *Combust. Flame* **2003**, *132*, 715−722.
(9) Schwer, D. A.; Lu P.; Green, W. H, Jr. *Combust. Flame* **2003**, *133*, 451−465.
(10) Fisher, E. M.; Pitz, W. J.; Curran, H. J.; Westbrook, C. K. *Proc. Combust. Inst*. **2000**, *28*, 1579−1586.
(11) Norton, T. S.; Dryer, F. L. *Proc. Combust. Inst*. **1990**, *23*, 179−185.
(12) Benson, S. W. *Thermochemical Kinetics*; John Wiley & Sons: New York, 1968; p 75.
(13) McEnally, C. S.; Pfefferle, L. D.; Mohammed, R. K.; Smooke, M. D.; Colket, M. B. *Anal. Chem*. **1999**, *71*, 364−372.
(14) McEnally, C. S.; Koylu, U. O.; Pfefferle, L. D.; Rosner, D. E. *Combust. Flame* **1997**, *109*, 701−720.
(15) McEnally, C. S.; Pfefferle, L. D. *Combust. Flame* **2004**, *136*, 155−167.
(16) Pitz, W. J.; Westbrook, C. K.; Curran, H. J. LLNL Combustion Chemistry Group, 2004; http://www-cms.llnl.gov/combustion/combustion-_home.html.
(17) O'Neal, H. E.; Benson, S. W. *J. Phys. Chem*. **1967**, *71*, 2903−2921.
(18) McMillen, D. F.; Lewis, K. E.; Smith, G. P.; Golden, D. M. *J. Phys. Chem*. **1982**, *86*, 709−718.
(19) Norfolk, S. D.; Taylor, R. *J. Chem. Soc., Perkin Trans. 2* **1976**, 280−285.
(20) Barnard, J. A.; Cocks, A. T.; Parrott, T. K. *J. Chem. Soc., Faraday Trans. 1* **1976**, *72*, 1456−1463.
(21) Glassman, I. *Proc. Combust. Inst.* **1988**, *22*, 295−311.
(22) Lias, S. G.; Bartmess, J. E.; Liebman, J. F.; Holmes, J. L.; Levin, R. D.; Mallard, W. G. *J. Phys. Chem. Ref. Data* **1988**, *17*, 1−861.
(23) Doute, C.; Delfau, J. L.; Akrich, R.; Vovelle, C. *Combust. Sci. Technol*. **1997**, *124*, 249−276.
(24) Wang, H.; Frenklach, M. *Combust. Flame* **1997**, *110*, 173−221.
(25) Pope, C. J.; Miller, J. A. *Proc. Combust. Inst*. **2000**, *28*, 1519−1527.
(26) McEnally, C. S.; Ciuparu, D. M.; Pfefferle, L. D. *Combust. Flame* **2003**, *134*, 339−353.